Sensitivity of chloride ingress modelling in concrete to input parameter variability

David Conciatori · Étienne Grégoire · Éric Samson · Jacques Marchand · Luc Chouinard

D. Conciatori
Ecole Polytechnique de Montréal, Montreal, QC, Canada e-mail: david.conciatori@polymtl.ca

É. Grégoire (&) É. Samson J. Marchand Simco Technologies Inc, 2666 boul du Parc-Technologique, suite 100, Quebec, QC G1P 4R7, Canada e-mail: egregoire@simcotechnologies.com

L. Chouinard
McGill University, Montreal, QC, Canada

Abstract The Rosenblueth point estimator method is used to propagate uncertainty on stochastic parameters in a multi-ionic reactive transport model for concrete degradation. The degradation mechanism that was analysed is the ingress of chlorides into concrete. This point estimator method is used because it requires a minimum number of simulations to compute means, standard deviations and skewness for the solution of the transport model. Two exposure cases are considered in this article: the first is a saturated case, and the second is an unsaturated case with wetting (4 days) and drying (3 days at 50 % relative humidity) cycles. The sodium chloride expo- sure during the wetting cycle of both cases was 500 mmol/L. In both cases, predictions from the model were compared to experimental results. The Rosenblueth approach yielded results comparable to Monte Carlo simulations for both saturated and unsaturated cases. The relative sensitivity of model parameters on prediction results are investigated through a sensitivity analysis. The sensitivity results show the high importance of ionic diffusion parameters and of exposure conditions, while the calculated initial mineral phases in the hydrated paste have lower importance.

Keywords Probabilistic chloride ingress · Multi- ionic reactive transport model · Corrosion initiation · Reinforced concrete

1 Introduction

Concrete structures worldwide are rapidly deteriorating and 20 % of repair costs are directly due to corrosion. Current statistics [2, 10, 32, 33] show that one out of nine bridges in the United States is rated as structurally deficient and that the average age of its 607,380 bridges is 42 years. The Federal Highway Administration (FHWA) estimates that to eliminate the backlog of deficient bridges by 2,028 would require annual investments of $20.5 billion while only $12.8 billion is being spent currently. In consequence, the number of bridges closed to traffic or with load restrictions is increasing. Reconstruction is not always the most cost-effective option in these cases, showing the need for better durability calculation tools.
The durability design guide for concrete structures of the European Union was outlined in the DuraCrete project [11]. It lays the general framework for the calculation of degradation mechanisms such as chloride ingress, carbonation, and cracking in terms of loading and resistance factors, taking into account the material, environmental, structural, and model uncertainty into the calculation. The DuraCrete chloride ingress model uses Fick's second law, and the simplifications necessary for its implementation brings about some weaknesses. It was demonstrated that simplified deterioration models are only applicable to idealized cases and can lead to erroneous results in real applications [20].

Reactive transport models dedicated to the prediction of chloride ingress in reinforced structures have become a central element of deterioration calculations for long-term service-life predictions [14]. Models have even became part of construction guides, such as the Unified Facilities Guide Specifications (UFGS) for US federal agencies (US Navy, US Army Corps of Engineer, US Air Force and NASA) [30]. While advanced models capable of calculating degradation of structural elements are available, they are rarely used in probabilistic analyses due to high computational demands. This paper will show that combining simplified probabilistic analyses with quantitative analysis of parameter variability allows for the calculation of loading parameters for durability analysis, compatible with durability analyses as outlined in the DuraCrete guide. A sensitivity analysis is first per- formed in order to quantify the importance on individual simulation variables on the output of the model. The probabilistic analysis is based on the Rosenblueth point estimators method [22, 23], and is validated by comparison with Monte Carlo modelling. The stochastic parameters in

the example presented are the material transport properties. They have been quantified and qualified in a recent article [7].

The remainder of the paper is organized as follows. In Sect. 2, a numerical model for ion transport in reinforced concrete is discussed, following by a brief description of the probabilistic and sensitivity methods. In Sect. 3, two application examples are presented. Both examples are based on laboratory test results on the same concrete for two different exposure conditions: immersion in salt water and wetting- drying cyclic exposure. Section 3.1 contains the specific of the concrete mixture used, and Sect. 3.2 details the exposure conditions of the specimens. Section 3.3 shows the results of the sensitivity analysis to determine the relative influence of model parameters on predictions, and Sect. 3.4 shows the results of the probabilistic analyses.

2 Methodology

A description of the service life model is presented in Sect. 2.1. This model was used to reproduce results of laboratory prepared concrete cylinders exposed to a chloride solution under both immersed and wetting- drying cycles. The sensitivity methodology used to analyse the variation in model output caused by initial parameter variation is presented in Sect. 2.2. The point estimator and Monte Carlo methodologies are presented in Sect. 2.3.

2.1 Model description

All numerical simulations presented in this paper were run using a finite element software called STADIUM. The software is a multi-ionic transport model based on a sequential split operator approach that separates ionic movement and chemical reactions. Details on the model can be found in [24–26]. The current version of the model accounts for both physical and chemical interactions. Physical chloride binding is modeled by a Freundlich isotherm and directly incorporated in the transport equations. All chemical reactions, including chloride binding due to formation of Friedel's salt, are treated by a separate chemical module.

The transport part is described by the extended Nernst-Planck equation applied to unsaturated materials subjected to temperature fluctuations. This equation accounts for the electrical coupling between ionic fluxes, chemical activity effects, transport of species due to water content gradient and temperature effects:

$$\rho\frac{\partial(c_i^b)}{\partial t}+\frac{\partial(wc_i)}{\partial t}-\mathrm{div}\left(D_i w\mathrm{grad}(c_i)+\frac{D_i z_i F}{RT}wc_i\mathrm{grad}(\psi)+D_i wc_i\mathrm{grad}(\ln\gamma_i)+\frac{D_i c_i\ \ln\ (\gamma_i c_i)}{T}w\mathrm{grad}(T)+c_i D_w\mathrm{grad}(H)\right)=0 \quad (1)$$

where c_i is the concentration [mmol/L], c^b is the chloride bound from physical interaction [mol/kg], w is the water content [m^3/m^3], q is the density of the material [kg/m^3], D_i is the diffusion coefficient [m^2/s], z_i is the valence number of the ionic species i, F is the Faraday constant [96488.46 C/mol], w is the electro- diffusion potential [V], R is the ideal gas constant [8.3143 J/mol/°K], T is the temperature [°K], c_i is the activity coefficient, and D_w is the water diffusivity [m^2/s]. Eight ionic species were considered for this study: OH^-, Na^+, K^+, SO^{2-}, Ca^{2+}, $Al(OH)^-$, H_2SiO^{2-} and Cl^-. The activity coefficients in the model are evaluated on the basis of the Harvie, Moller and Weare (HMW) implementation of Pitzer's ion interaction model [35].

The physical binding term was estimated from binding experiments performed on hydrated C_3S pastes exposed to different chloride concentrations. This term is zero for all ionic species except chloride, for which c^b is given by:

$$c_{Cl}^b=\xi\times p\,c_{Cl}^u \quad (2)$$

where n is a conversion factor involving the amount of C-S-H in the material that changes the isotherm estimated in units of [mol_{Cl}/kg_{dry} C_3S] into [mol/ $kg_{material}$], and p and u are fitting parameters. The binding experiments were performed at two different pH conditions: [OH^-] = 40 and 435 mmol/L. A linear interpolation between these two values allows esti- mating the physical binding at any pH. The linear variation was assumed since only two data sets were available for analysis.

The electrodiffusion term in Eq. (1), involving the potential w, is mainly responsible for maintaining the electroneutrality of the pore solution. Its role is to balance each individual ionic mobility so that there is no net accumulation of charge at any location in the pore solution. In cementitious materials, where pore solution concentrations are high (pH in the range 13– 14, [1]), this term can have a significant influence on the ingress rate of

contaminants (see for instance [26], that discusses sulfate attack mechanisms). To solve the diffusion potential w, the ionic transport equation is coupled to Poisson's equation, which relates the electrodiffusion potential in the material to the ionic profile distributions:

$$\mathrm{div}(\tau_s w \mathrm{grad}\psi) + \frac{F}{\epsilon} w \left(\sum_{i=1}^{N} z_i c_i \right) = 0 \tag{3}$$

where ε [6,9 × 10^{-10} C/V/m] is the permittivity of water, s_s is the intrinsic tortuosity of the material (described later) and N is the number of ions in the pore solution.

To account for moisture flow induced by capillary potential gradients in unsaturated materials, the previous equations are coupled to:

$$\frac{\partial w}{\partial H}\frac{\partial H}{\partial t} + \frac{\partial w}{\partial T}\frac{\partial T}{\partial t} - \mathrm{div}\left(D_H \mathrm{grad}(H) + D_T \mathrm{grad}(T)\right) = 0 \tag{4}$$

where H [–] is the relative humidity (RH), and D_H [m^2/ s] and D_T [m^2/s/K] are the moisture transport coefficients, given by:

$$D_H = \frac{k_s k_r^l \rho_l R}{\mu M_w}\frac{T}{H} + \frac{\theta_g \tau_s \tau_r^g D_v^o M_w}{\rho_l R}\frac{p_v^s}{T} \tag{5}$$

$$D_T = \frac{k_s k_r^l \rho_l R}{\mu M_w}\left(\ln(H) - \frac{T}{p_v^s}\frac{\mathrm{dp_v^s}}{\mathrm{dT}}\right) - \frac{\theta_g \tau_s \tau_r^g D_v^o M_w}{\rho_l R}\frac{H}{T^2} p_v^s \tag{6}$$

where k_s [m^2] is the intrinsic permeability of the saturated material, k_r^l [–] is the relative permeability of the liquid phase, ρ_l [kg/m^3] is the liquid phase density, μ [Pa.s] is the dynamic viscosity of the liquid phase, M_w [0.018 kg/mol] is the molar mass of water, θ_g [m^3/ m^3] is the volumetric gas phase content, D_v^o [m^2/s] is the vapor self-diffusion coefficient, p_v^s[Pa] is the saturation vapor pressure, and τ_r^g [–] is the relative tortuosity of the gaseous phase.

The terms $\partial w/\partial H$ and $\partial w/\partial T$ in Eq. (4) are associated with the moisture isotherm of the material. In the present study, the moisture is estimated by a model which accounts for the measured saturation level of the material when in equilibrium at 50% RH (S_{50}).

Finally, the temperature distribution in the material is calculated from the classical heat condition Eq. [25]:

$$\rho C_p \frac{\partial T}{\partial t} - \mathrm{div}(\kappa \mathrm{grad}(T)) = 0 \tag{7}$$

where ρ is the density of the material [kg/m^3], C_p is the specific heat of the material [J/kg/ºC], and k is the heat conductivity [W/m/°C]. For the purpose of this paper, all calculations were performed assuming that the material was maintained at a constant temperature.

The key material parameter that determines the rate of ingress of chloride and other contaminants in the structure is the diffusion coefficient D_i (see Eq. (1)). This parameter is influenced by many factors:

$$D_i = D_i^o \times \tau \times S(w) \times G(T) \times H(t) \times M(\phi) \tag{8}$$

where D_i^o is the diffusion coefficient of ion i in freewater [m^2/s] at a reference temperature T^{ref}, usually around 23ºC. Values for D_i^o can be found in textbooks or papers (e.g. reference [19]). The parameter τ is the intrinsic tortuosity of the material [25]. It can be evaluated from migration test results [27]. It usually corresponds to the measurement at 28 days of curing. The various functions affecting the diffusion coefficient are given as:

$$S(w) = S^{6.0} \tag{9}$$

$$G(T) = e^{0.028(T - T^{ref})} \tag{10}$$

$$H(t) = \frac{a}{1 + (a-1)e^{-\alpha(t-t^{ref})}} \tag{11}$$

$$M(\phi) = \frac{e^{4.3\phi/V_p}}{e^{4.3\phi_o/V_p}} \tag{12}$$

where S is the saturation level in pores, $ø_o$ is the initial porosity of the material, $ø$ is the porosity at time t and V_p is the volumetric paste content of the cementitious material [m^3/m^3]. The function $S(w)$ models the influence of the water content on diffusion. It is based on data found in [18]. The function $G(T)$ considers the effect of temperature [24, 35] on transport properties, compared to a reference value evaluated at the temperature T^{ref}. The function $H(t)$ takes into account the variation of the tortuosity as a result of the cement hydration process [25]. The transport properties of cementitious materials are generally high at young age but tend to decrease with time, especially when supplementary materials such as fly ash are used in the production of concrete. The reduction rate is determined by the factor a while the ultimate value of $H(t \to \infty)$, when the hydration process is completed, is given by a. Finally, the alteration to the material's microstructure caused by the chemical reactions between the external contaminants, such as sulfate, and the cement paste can induce local porosity variations that affect the diffusion coefficients. This is taken into account using the feedback function $M(ø)$, which was established on the basis of porosity and diffusion coefficient measurements performed over a wide range of cementitious materials [25]. The porosity variations are calculated by accounting at each node for changes in the solid phase distribution evaluated at the previous time step. The description of the chemical module is given below. The water diffusivity, which governs the kinetics of moisture transport in the materials, is also affected by the feedback function.

Eight ionic species are considered in the model, giving 11 variables in the system of equations: 8x c_i, ψ, w, and T, which are solved using 8 ionic conservation Eq. (1), coupled with Eqs. (3)–(7). This system of nonlinear equations is solved using the Newton- Raphson method with all equations solved simultaneously. The spatial discretization of this coupled system is based on the finite element approach using the standard Galerkin procedure. An Euler implicit scheme is used to discretize the time-dependent part of the model. The numerical details are given in reference [25].

The second module in STADIUM consists in a chemical equilibrium code. Following the transport step, the chemical equilibrium module verifies, at each node of the mesh, the equilibrium between the concentrations and the solid phases of the hydrated cement paste, e.g. calcium hydroxide, calcium silicate hydrates, ettringite, and monosulfates. The equilibrium of each phase is modeled according to:

$$K_m = \prod_{i=1}^{N} c_i^{\nu_{mi}} \gamma_j^{\nu_{mi}} \qquad \text{with} \qquad m = 1, \ldots, M \tag{13}$$

where M is the number of solid phases, N is the number of ions, K_m is the equilibrium constant (or solubility constant) of the solid m, c_i is the concentration of the ionic species i, γ_i is its chemical activity coefficient, and υ_{mi} is the stoechiometric coefficient of the ith ionic species in the mth mineral. If the solution is not in equilibrium with the paste, solid phases are either dissolved or precipitated to restore equilibrium. The pore solution is thus adjusted to enforce the equilibrium relationships (13) of the mineral phases. Solid phases can also be formed when aggressive species penetrate into the porous network of the material, e.g. ettringite, gypsum, hydrated sodium sulfate, and halite.

After the pore solution concentrations are modified, the solid phases are also corrected according to:

$$S_m^t = S_m^{t-1} - wX_m\Gamma_m/\rho \tag{14}$$

where S_m is the amount of a given solid phase [g/kg of material], t indicates the time step, Γ_m is the molar mass of the solid m [g/mol], X_m represent the amount of a given solid phase that has to dissolve to reach equilibrium, and ρ is the density of the saturated, wet material [kg/m^3].

Some solid phases do not act as pure mineral but instead form solid solutions. This is the case for the formation of the chloride-AFm solid compound called Friedel's salts, which is the main reaction product formed upon chloride penetration in cementitious materials [13]. In the present study, it was considered that Friedel's salts form solid solutions with two AFm phases: monosulfate and C_4FH_{13}. The equilibrium is calculated by assuming that AFm end-members monosulfate and C_4FH_{13} act as pure minerals and that Friedel's salts follow the relationship:

$$K_{ss} = \frac{(\mathrm{Cl})^{|z|}}{(c_{\mathrm{AFm}})} \frac{\chi_{\mathrm{AFm}}}{\chi_{\mathrm{Friedel}}} f_{ss} \tag{15}$$

where K_{ss} is the equilibrium constant of the solid solution, (Cl) is the activity of chloride in the pore solution [mmol/L], (c_{AFm}) is the activity of the exchanging species in the AFm end-member [mmol/ L], z is the valence number of this species, χ_{AFm} represents the mole fraction of the AFm end-member [mol/kg of material], χ_{Friedel} represents the mole fraction of the Friedel's salt end-member [mol/kg of material], and f_{ss} [–] is a correction factor that accounts for the nonideality of the solid solution.

The equilibrium constants of solid phases considered in the chloride ingress simulations are presented in Table 1. The equilibrium relationships were expressed on the basis of the species listed below Eq. (1).

Table 1 Equilibrium constants of solid phases

Mineral phases	log K_m
Portlandite (CH)	−5.15
CaH_2SiO_4	−8.16*
Monosulfate (AFm)	−29.40
Ettringite (AFt)	−44.00
C_4FH_{13}	−29.40
Solid solutions	**log K_{ss}****
Friedel's salt (from monosulfate)	3.0
Friedel's salt (from C_4FH_{13})	−1.0

* K_{sp} ¼ *f* ðC=SÞ for C–S–H [5]

** Incorporates the nonideality correction factor

2.2 Sensitivity methodology

The sensitivity analysis of the model was based on the calculation of the elasticity of the model parameters. The elasticity provides an estimation of the relative importance of variations of parameters on the output of a model [9]. It is calculated as:

$$\eta = \frac{\triangle Y}{\triangle P} \frac{\overline{P}}{\overline{\overline{Y}}} \tag{16}$$

where Y is the output of the model calculated with parameters P and ΔY is the variation in the output of the model with input parameter variation of ΔP. In this study, the value of ΔP used was 1 %. Different values of ΔP are likely to yield different elasticity values. The value of ΔP chosen in this study analyzes the sensitivity of the model near the mean of the output distribution. A similar sensitivity methodology called the sensitivity ratio is described in [31]. The output of the model that was tracked for the sensitivity analysis is the total chloride content, which is the sum of chlorides in the pore solution and bound to the paste. This value is used when determining the risk of corrosion initiation of steel rebar in concrete elements subjected to chloride exposure [26].

Three categories of parameters are considered in the sensitivity analysis. The first category contains the transport properties of concrete: volume of permeable voids (ø), ionic diffusion coefficient (D_{OH}), and water permeability (k). They are known to contain uncertainty based on the intrinsic heterogeneity of concrete, as well as the laboratory testing methods for their determination, and numerical methods necessary to derive the values from the laboratory testing. The second category contains the physical and chemical properties of the binder and the solid phases formed during the hydration of concrete: the binder density, and the portlandite, CaH_22SiO_4, and monosulfate content. The third category contains the exposure conditions, which define the boundary conditions of the simulation: the NaCl content of the exposure solution, the temperature, and the relative humidity of the drying exposure cycle.

2.3 Probabilistic methodology

The propagation of uncertainty in an iterative, non- linear finite element models through algebraic manipulation is not

feasible. Numerical integration methods or Monte-Carlo modelling is possible, however it is very computationally expensive [6]. An alternative is using point estimators to calculate the statistical moments of the model output, based on the variability of the input parameters. When using appropriate point estimators, such as the Rosenblueth point estimators, the statistical moments of the model response can be calculated [22, 23]. The first three statistical moments of a distribution are the mean, variance, and skewness, which respectively give the location, spread, and asymmetry shape of a distribution. We will show that these statistical moments contain enough information to approximate the complete distribution of variability of the model output. We will also compare the results of these approximations with Monte-Carlo validations.

The probabilistic modelling of chloride ingress is performed using the STADIUM modelling software that was presented in the previous section. This modelling is performed by taking into account the direct dependence of the transport variables, as explained in [7].

2.3.1 Monte Carlo modelling

Monte Carlo modelling is used, in this case, to generate the complete probability distribution of the outputs of the model based upon the statistical distribution of the input variables. A random number generator is used to generate values for the input transport properties that are to be considered probabilistic. Then, a simulation is run with these values, and the model response is stored. This methodology is employed multiple times until the response shape of the simulations results distribution is stable.

In the current case, the model response was studied after three and six months of exposure, for which experimental data were available (see Sect. 3.2). Four transport properties where considered as probabilistic. The Monte Carlo testing was stopped when the variations in the mean and in the standard deviation of the chloride content varied by less than 0.1% at any point over the depth of the simulated element. This required ~1,000 simulations for each exposure case. On a computer equipped with an x86 Core i5 processor, this required a combined 2 weeks of computation time.

2.3.2 Rosenblueth point estimators method

In the current study, the Rosenblueth point estimators [22, 23] were used. The Rosenblueth point estimators method discretizes the distribution of input variables at specific points. These discrete points are a function of the statistical moments of the input variables.

Considering a real function Y of a real variable X, it can be shown [23] that the estimation of the mean, standard deviation and skewness of Y (respectively, Y, S_y, and γ_y) can be calculated from point estimators of X, independently of the distribution of the variable. The point estimators of X (x_+ and x_- with respective probability mass p_+ and p_-) must be calculated to account for the statistical properties of X (X, S_x, and γ_x) and are calculated as:

$$x_+ = \overline{X} + \xi_+ S_x \tag{17}$$

$$x_- = \overline{X} - \xi_- S_x \tag{18}$$

$$p_+ = \frac{\xi_-}{\xi_+ + \xi_-} \tag{19}$$

$$\xi_- = \xi_+ - \gamma_x \tag{20}$$

where

$$\xi_+ = \frac{\gamma_x}{2} + \sqrt{1 + \left(\frac{\gamma_x}{2}\right)^2} \tag{21}$$

$$\xi_- = \xi_+ - \gamma_x \tag{22}$$

account for the skewness of the distribution of X. If the function Y is multivariate, this is repeated for each variable X_k.

Solving Y for each combination i of point estimators of X_k, the statistical moments of Y are:

$$\overline{Y} = \sum_{i=1}^{c} P_i \, y_i \tag{23}$$

$$S_y = \sqrt{\sum_{i=1}^{c} P_i (y_i - \overline{Y})^2} \tag{24}$$

$$\gamma_y = \sum_{i=1}^{c} \frac{P_i (y_i - \overline{Y})^3}{S_y^3} \tag{25}$$

where c is the number of possible combinations of point estimators of v variables ($c = 2^v$), and:

$$y_i = f(x_{1\delta}, x_{2\delta}, \ldots x_{v\delta}) \tag{26}$$

$$P_i = \prod_{k=1}^{v} p_{k\delta} \tag{27}$$

where δ is the sign of the point estimator as defined in Eqs. (17) through (19). Here, P_i is the probability associated with a combination of transport properties, and y_i is the simulation result associated with transport properties $x_{k\delta}$. With four properties considered as probabilistic, the Rosenblueth point estimators methodology requires 16 simulations, which is advantageous when compared to ~1,000 for the Monte Carlo methodology.

3 Case study

Concrete specimens were exposed in chloride solutions of known concentrations for three and six months in both immersed and cyclic conditions. Independently, the transport properties of the same material were measured with the methods described in [7]. Chloride content profiles measured on the specimens after 3 and 6 months were compared to probabilistic simulations results based on the methodology described in Sect. 2.3. The sensitivity methodology, as described in Sect. 2.2 was applied to the same exposure conditions, but the results were analysed over a longer period of 10 years. The sensitivity analysis is performed first to determine the most sensitive modelling parameters to consider for the probabilistic analysis.

3.1 Concrete specimens

The concrete mixture used in this study was batched in a laboratory setting using a 80 l planetary mixer. Test specimens were cast in standard ø100 × 200mm^2 cylinders, demolded after 24 h and cured in limewater for 28 days. The transport properties, concrete proportions, binder composition, calculated initial phases and pore solutions are detailed in Table 2.

3.2 Exposure conditions

Chloride ponding tests were started on concrete samples after curing in limewater. The tests specimens were standard concrete cylinders that were cut in half. All faces were sealed with epoxy coating except the cut face, which was exposed to the solution.

The chloride ponding was performed using a modified version of the ASTM C1542 procedure [4]. This standard calls for a concrete slab with an exposed face of dimensions no less than 0.03 m^2, where a standard concrete cylinder has a surface of ~0.0078 m^2. Additionally, the specimens are immersed in the exposure solution instead of ponded on the exposed surface. This second modification improves the concentration stability of the solution because of the greater volume which diminishes variations due to evaporation.

The immersion solution used was a 3% sodium chloride (NaCl) aqueous solution, which is equivalent to a concentration of 500 mmol/L. Two exposure durations were scheduled: 3 and 6 months. The solution was renewed regularly to maintain stable concentrations.

In addition to the immersion testing, a cyclic chloride ponding test was also performed. The wetting cycle had identical conditions to the immersion testing for a duration of 4 days, followed by 3 days of drying in laboratory ambient conditions. The laboratory temperature was maintained at 23 ± 2°C. The humidity was 50% on average.

Table 2 Concrete properties for the sensitivity and probabilistic modelling

Property	Unit	Value
Transport properties		
Volume of permeable voids (✓)	%	12.40
Ionic diffusion coefficient (D_{OH})	E-11 m^2/s	10.37
Saturation in 50 % humidity ($S_{50\ \%}$)	(ratio)	0.44
Water permeability (k)	E-22 m^2	12.77
Concrete proportions		
w/b	(ratio)	0.40
Cement	kg/m^3	390
Water	kg/m^3	156
Coarse aggregates (0.8–5mm)	kg/m^3	1,000
Fine aggregates (5–20mm)	kg/m^3	790
Air entrainer	ml/m^3	25
Binder composition (GU cement)		
CaO	%*mass*	62.80
SiO_2	%*mass*	19.90
Al_2O_3	%*mass*	4.70
Fe_2O_3	%*mass*	2.80
SO_3	%*mass*	2.12
MgO	%*mass*	2.58
K_2O	%*mass*	0.89
Na_2O	%*mass*	0.28
TiO_2	%*mass*	0.19
P_2O_3	%*mass*	0.23
LOI	%*mass*	2.88
Initial solid phases		
Portlandite (CH)	*g/kg*	54.4
CaH_2SiO_4	*g/kg*	51.9
Monosulfate (AFm)	*g/kg*	24.7
C_4FH_{13}	*g/kg*	4.4
Initial pore solution		
$Na^þ$	*mmol/L*	155.0
$K^þ$	*mmol/L*	351.0
OH^-	*mmol/L*	506.0

In order to measure the chloride penetration, powder samples were extracted by dry milling after each exposure period (3 and 6 months). The samples were extracted at small increments from the exposed surface of the specimens down to about 40 mm. This procedure is detailed in the ASTM C1152 standard procedure [3]. Two specimens were tested after each exposure duration, for the two exposure cases.

3.3 Sensitivity analysis

The goal of the sensitivity analysis is to quantify the influence of parameter variations. For the sensitivity study, 10 different simulation properties were considered individually. Table 3 shows the baseline value and sensitivity values for these properties, along with the ΔP value for the calculation of the parameter elasticity. The parameter elasticities highlight the influence around the mean of each parameter on the chloride concentration results. An elasticity of 1% indicates that a variation of input parameter value will induce an equal variation in model output. If the elasticity is less than 1%, its influence on model output will be reduced, whereas if it exceeds 1%, its influence will be greater. A negative elasticity indicates that an increase in input parameter value will decrease the model output.

Table 3 Parameter variations considered in sensitivity analysis

Property	Unit	Base value ($\overline{P}$)	Sensitivity value ($\overline{P} + \Delta P$)	Change ΔP
Volume of permeable voids (ø)	%	12.40	12.52	0.97%
Ionic diffusion coefficient (*DOH*)	E-11 m^2/s	1.037	1.047	0.96%
Water permeability (k)	E-22 m^2	1.277	1.290	1.02%
Saturation in 50% Relative Humidity ($S_{50\%}$)	(ratio)	0.44	0.444	1.00%
Binder density (q)	kg/m^3	3140.0	3,171.4	1.00%
Portlandite (CH)	g/kg	54.40	54.94	0.99%
Calcium sillicate (CaH_2SiO_4)	g/kg	51.90	52.42	1.00%
Monosulfate (AFm)	g/kg	24.70	24.95	1.00%
Sodium chloride exposure (NaCl)	mmol/L	500	505	1.00%
Temperature (T)	°C	20.0	20.2	1.00%
Drying cycle relative humidity (RH)	%	50.0	50.5	1.00%

3.3.1 Sensitivity after 10 years

The elasticity of each parameter was plotted over the simulation depth after 10 years of exposure. Figure 1 shows the results of the immersed case, and Fig. 2 shows the results of the wetting/drying cycle case. The finite element mesh used for the simulations had 61 nodes and 60 elements. The elements had varying widths, with finer elements near the surface. The results have been plotted as the average elasticity of five adjacent finite element nodes for clarity.

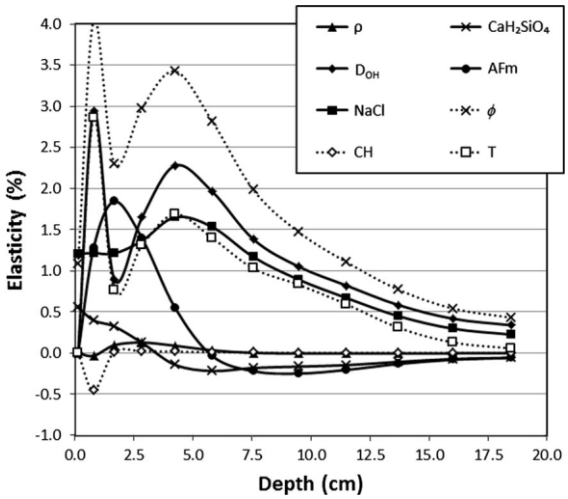

Fig. 1 Mean elasticity of each parameter after 10 years of exposure over the simulation depth, for the immersed case

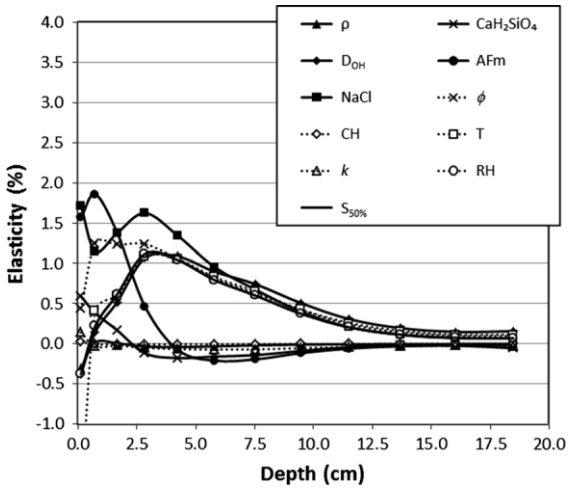

Fig. 2 Mean elasticity of each parameter after 10 years of exposure over the simulation depth, for the wetting-drying case

The elasticity of most parameters is greater and more variable near the exposed surface, and stabilizes deeper in the concrete element. At the end of a 10-year simulation, the elasticity of the volume of permeable voids, ionic diffusion coefficient and temperature is higher for the wetting-drying cycle exposure than for the immersed case. Other parameters have comparable elasticities, and water permeability, relative humidity and saturation in 50% relative humidity are only applicable for the wetting-drying exposure.

3.3.2 Sensitivity near corrosion initiation threshold

For engineering applications, the total chloride content is tracked in these finite element simulations to calculate the time to reach the corrosion initiation threshold at the depth of the rebar. This chloride threshold varies in the literature, from 0.3 to over 2.0% of total chlorides by weight of cement [15]. The lower threshold of 0.3% is specified by the FHWA as the content at which corrosion is likely to initiate for normal black steel bars in concrete [21]. A threshold of 0.5% is reported in the literature [15] as the mean concentration of corrosion initiation.

While the previous section shows that the elasticity of simulation parameters varies over the depth of the simulated

concrete element, the elasticity where the chloride content profile reaches the corrosion initiation threshold is notably stable over time. To analyse this phenomenon, we track the location where the baseline simulation reaches the initiation threshold over the simulation duration. We then compare the sensitivity simulations output to the baseline value at this position over time. Figure 3 shows the elasticity of the 10 parameters in the wetting-drying exposure case, over time, at the location where the baseline simulation reaches the FHWA threshold of 0.3% total chlorides by weight of cement. This figure shows the stability of the sensibility at the corrosion threshold over time. In this specific simulation, the corrosion initiation threshold reaches a depth of 1.7 cm after 1 year, 5.2 cm after 5 years, and 7.7 cm after 10 years. The immersed exposure simulations show similar stability, as does the analysis considering a threshold of 0.5% total chlorides by weight of cement reported in the literature.

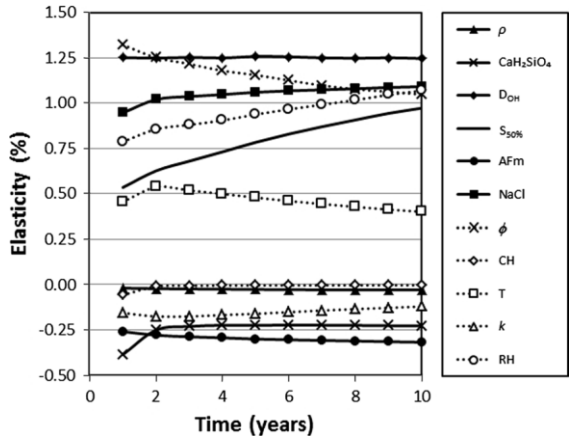

Fig. 3 Elasticity over time at depth where baseline simulation reaches the chloride threshold of 0.3 % total chlorides by weight of cement

In light of this apparent stability of parameter elasticity near the corrosion initiation threshold, further analyses will focus on the mean elasticity over the simulation duration of 10 years. Figure 4 shows the mean elasticity of these simulation parameters for two different thresholds (0.3 and 0.5 % total chlorides by weight of cement) and for the two exposure cases. The elasticity indicated is the mean change of the total chloride content caused by a 1.0 % change in the indicated simulation parameter over the 10-year simulation duration. The range indicated is the variation (minimum and maximum values) of elasticity that are measured at the depth of the chloride thresholds over the entire simulation duration.

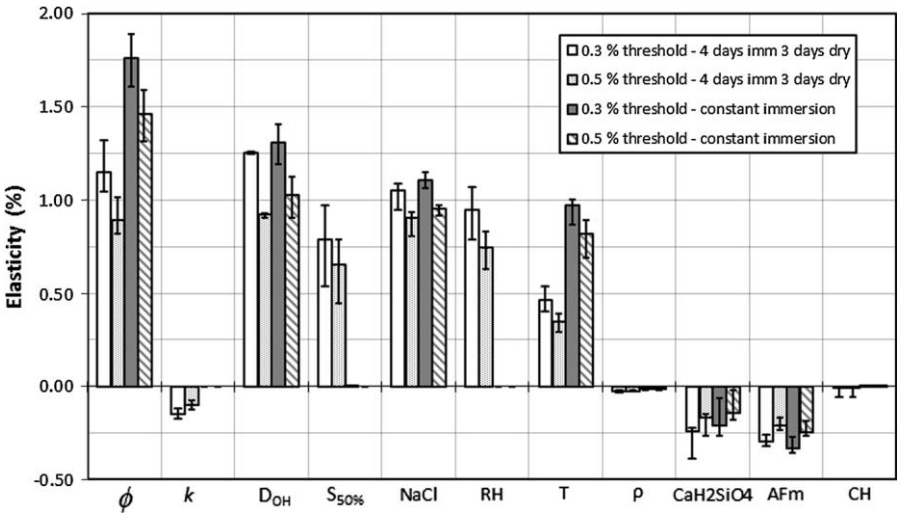

Fig. 4 Mean elasticity of each parameter for each exposure case and chloride initiation threshold indicated (as % of cement mass), with range of variation indicated

The results in Fig. 4 show similar conclusions than those discussed in Sect. 3.3.1. One exception is the monosulfate content, which has low negative elasticity near the chloride threshold, but has higher positive elasticity near the surface of the concrete element (see Figs. 1 and 2). Monosulfate is directly connected to the binding capacity of the chloride

ions in the cement paste [16, 28]. Thus, an increase in monosulfate content in concrete will increase the capacity of the material to bind chlorides near the surface, explaining the high positive elasticity in depths up to 5 cm after 10 years. Since chlorides bound to the cement paste are isolated from the pore solution, they will not diffuse deeper in the concrete element, leading to lower monosulfate elasticity deeper than 5 cm.

The volume of permeable voids and ionic diffusion coefficient both have similar mean elasticities of around 1.0 up to 1.5% for the permeable voids for the constant immersion case. The saturation ratio in 50% relative humidity shows a mean elasticity of 0.5 to 0.75%, depending on the threshold. The water permeability elasticity is much lower at around −0.15%. The short duration of the drying period (3 days) may have reduced the elasticity of the water permeability parameter. Further analysis will be necessary for the simulation of concrete elements with longer drying periods. The water permeability, relative humidity and saturation in 50% relative humidity parameters have no influence for the constant immersion exposure. The elasticity of the exposure concentration is close to 1.0% for both exposures. The elasticity of the temperature for the constant immersion exposure is twice that of the wetting/drying exposure. As implemented in the service life prediction model, the sensitivity of the binder density is less than −0.03%, and the sensitivity of the initial portlandite content less than −0.01%. Both CaH_2SiO_4 and monosulfate initial content have elasticities of −0.15 to −0.30% near the corrosion initiation threshold.

It should be noted that both the relative humidity and saturation ratio in 50% relative humidity have slightly increasing elasticity over time near the corrosion initiation threshold. It should also be noted that the measured elasticities have been calculated with variations close to the mean of the parameters, with a range of ~1%. This methodology can also be applied in cases where larger variations in parameters have to be accounted for.

3.4 Probabilistic analysis

Probabilistic simulations with the model described in Sect. 2.1 were carried out with the two methodologies described in Sect. 2.3. The stochastic variables considered in the probabilistic analysis are summarized in Table 4. The coefficient of variations and distributions functions are taken as the maximum observed results in [7].

Table 4 Variability and distribution of transport properties considered in probabilistic analysis

Transport property	COV	Distribution
Volume of permeable voids ($ø$)	4 %	Normal
Ionic diffusion coefficient (DOH)	24 %	Lognormal
Saturation in 50 % humidity ($S_{50\%}$)	8 %	Normal
Water permeability (k)	37 %	Normal

These parameters are considered either because they show high sensitivity (Volume of permeable voids, Ionic diffusion coefficient, Saturation in 50% relative humidity) or because they exhibit high variability (Water permeability). Other parameters that exhibited high sensitivity were environmentally controlled parameters and their variability was negligible (NaCl exposure content, Relative humidity of drying cycle, Temperature).

A qualitative analysis of the chloride content distribution results of the Monte Carlo analysis at varying depths over the simulation duration was performed. A general assessment using quantile–quantile plots (the methodology for which is outlined in [7]) indicated that the distribution best fitted to the total chloride content was a Gamma distribution over most of the chloride content profile.[1] The shape (a) and scale (β) parameters are estimated with the matching moments method [12]:

$$\alpha = \left(\frac{\overline{Y}}{S_y}\right)^2 \tag{28}$$

$$\beta = \left(\frac{S_y^2}{\overline{Y}}\right) \tag{29}$$

where Y and S_y are taken from Eqs. 23 and 24. The skewness of the moments obtained from the Rosenblueth point estimators method in Eq. 25 was compared to skewness the estimated gamma distribution ($c = 2/\alpha^{0.5}$). This comparison confirmed the qualitative assessment of the quantile - quantile plots. From the a and β parameters, the complete shape of the probability distribution function of the estimated gamma distribution can be calculated. In turn, this probability

distribution function will be compared to the Monte Carlo results.

To compare the results of the Monte Carlo and the Rosenblueth points estimators simulations, we analyze the 95% confidence interval by comparing the 2.5 and 97.5% percentiles of the distributions. Figure 5 shows the probabilistic results after 3 and 6 months of exposure for the immersed case. Figure 6 shows the results after the same exposure times for the 4 days wetting / 3 days drying case. The simulation results are shown with the 95% confidence interval of both probabilistic analyses. For validation, the total chloride content of the laboratory specimens are also shown. The analysis of chloride concentration in the specimens is made on concrete powder extracted at regular intervals over a depth of 2.5 mm. Chloride concentration measurements are thus an average concentration over this depth. The range indicated on the experimental validation points shows the approximate thickness of the milling from which the powder specimen was taken.

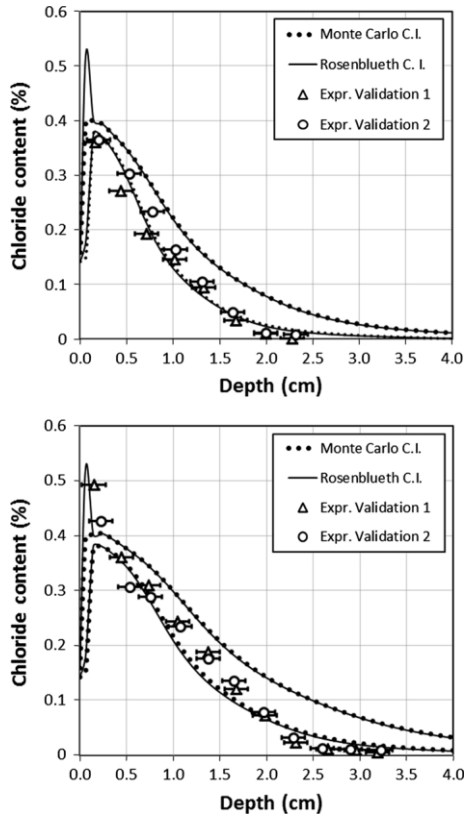

Fig. 5 95 % Confidence interval of chloride content prediction with Rosenblueth points estimators, with Monte Carlo verification, and experimental chloride profile points of laboratory specimens for immersed case after (*top*) 3 months, and (*bottom*) 6 months—the range indicates the thickness of the milling from which the powder sample was taken

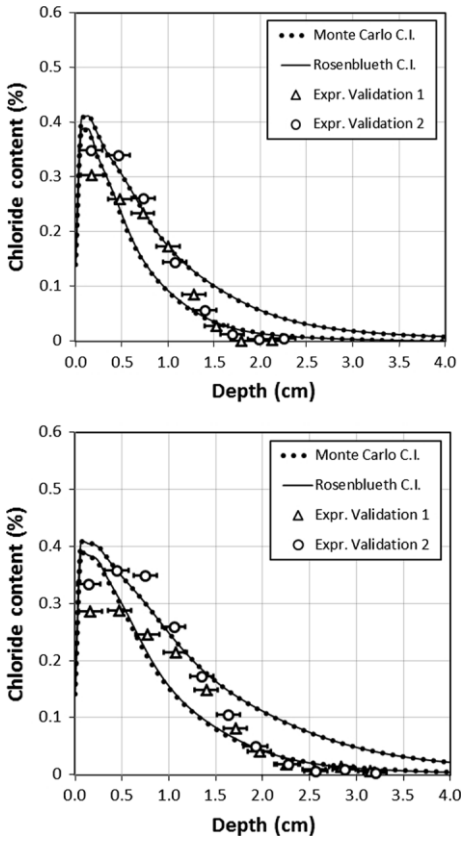

Fig. 6 95 % Confidence interval of chloride content prediction with Rosenblueth points estimators, with Monte Carlo verifica- tion, and experimental chloride profile points of laboratory specimens for wetting-drying case after (*top*) 3 months, and (*bottom*) 6 months—the range indicates the thickness of the milling from which the powder sample was taken

In addition, the difference between the confidence interval bounds calculated from the Rosenblueth point estimators and the Monte Carlo results has been calculated. The maximum positive, maximum negative, and average absolute differences between the Monte Carlo and Rosenblueth point estimator methodologies are indicated in Table 5.

For the immersed exposure case, the maximum positive difference for both 2.5 and 97.5% percentiles is at the second element of the finite element mesh (situated at 0.6 mm), as seen in Fig. 5. This high local difference (peak value in Table 5), which is not typical of the rest of the results, is caused by a difference in the depth of the degradation front in simulations for which the point estimator combination leads to higher transport properties.

Cover concrete can be divided into two zones (1) the concrete skin, which accounts for the first few millimeters (generally under 5 mm) of cover, where the concrete properties change drastically [17], and (2) the breathing zone,

where large fluctuations are recorded balancing with the environmental boundary conditions in cases where concrete is affected by wetting and drying cycles [8, 29]. The concrete skin is affected whether concrete is exposed to drying cycles or not, since this layer is mainly characterized by the dissolution of the portlandite phase, leading to conditions similar to the border element (at x = 0 mm) for elements that the degradation front has reached.

Table 5 Maximum positive, maximum negative, and average absolute difference (in chloride content (%)) between the confidence interval bounds (CIB) of the estimated gamma distribution from the Rosenblueth point estimators and Monte- Carlo method

Percentile	3 months		6 months	
	2.5%	97.5%	2.5%	97.5%
Immersed				
Max. pos. diff.	0.030	0.124*	0.030	0.125*
Max. neg. diff.	−0.007	−0.003	−0.008	−0.003
Avg. abs. diff.	0.002	0.003	0.002	0.003
Cyclic				
Max. pos. diff.	0.007	0.002	0.008	0.002
Max. neg. diff.	−0.001	−0.002	−0.001	−0.002
Avg. abs. diff.	0.001	0.000	0.001	0.000

* peak value

The peak variations observed in the simulations of the immersed case are caused by the difference in depth of the concrete skin between the simulations using different points estimators. In this specific example, 8 of the 16 immersed simulations using point estimators resulted in the first and second elements being in the concrete skin zone, and the other 8 simulations had only the first element in the concrete skin zone. This was observed after both 3 months and 6 months of exposure.

This change in model response leads to very different chloride content at the second element between simulations, which leads to a higher calculated standard deviation when calculated with Eq. (24). The phenomenon was studied in geotechnical mixed behaviour models using a version of the Rosenblueth points estimators [34]. In the current application, this behaviour is observed only in the first 2 elements of the 61-node finite element mesh, where the elements are very dense, and not the concrete core where steel rebar are generally placed. Additionally, this behavior does not affect the mean of the probability density of the model results. This phenomenon is thus not a concern for long-term service life simulations.

4 Conclusion

A methodology for the calculation of relative importance of parameters in service life studies of concrete elements was presented. In addition, a probabilistic methodology based on the statistical moments of the input parameters was presented and was compared to a Monte-Carlo validation study. Both methodologies were applied to a case study of laboratory-prepared samples that were exposed to chloride ponding tests of two different durations.

The sensitivity analysis of the presented case studies shows the important influence of the ionic diffusion parameters and of the exposure conditions during service-life simulations. Additionally, exposure conditions containing wetting and drying cycles influence the sensitivity of the volume of permeable voids and temperature. Other parameters have similar sensitivity whether the conditions contain drying cycles or not. The sensitivity of most parameters was found to be stable around the corrosion initiation threshold for total chloride content found in the literature. This stability is of importance for engineering calculations of service-life for structures in aggressive environments, since the influence of changes in material design on the time to initiate corrosion can be quickly estimated from one set of results.

The Rosenblueth point estimator method presented in this paper provides an attractive option for the analysis of variability for advanced service-life forecasting models. It allows the determination of loading curves for reliability analyses and durability design, such as outlined in the DuraCrete report, at 1.6% of the computing cost of Monte-Carlo modelling. The probabilistic analysis of chloride content was shown to be comparable to Monte Carlo modelling, and was able to reproduce results from laboratory-prepared samples for two exposure cases and two exposure durations.

References

1. Anstice D, Page C, Page M (2005) The pore solution of carbonated cement pastes. Cement Concrete Res 35:377–383
2. ASCE, A.S.o.C.E.: 2013 report card for americas's infrastructure—bridges (2013). http://www.infrastructurereport card.org/a/documents/Bridges.pdf. Accessed 03 Dec 2013
3. ASTM-C1152: ASTM standard C1152, 2004 (2004) Stan- dard test method for acid-soluble chloride in mortar and concrete. ASTM International, West Conshohocken
4. ASTM-C1543: ASTM standard C1543, 2010 (2010) Standard test method for determining the penetration of chloride ion into concrete by ponding. ASTM International, West Conshohocken
5. Berner U (1992) Evolution of pore water chemistry during degradation of cement in a radioactive waste repository environment. Waste Manag 12:201–219
6. Conciatori D, Brühwiler E, Morgenthaler S (2009) Calculation of reinforced concrete corrosion initiation probabilities using the rosenblueth method. Int J Reliab Saf 3(4):345–362
7. Conciatori D, Grégoire E, Samson E, Marchand J, Chouinard L (2013) Statistical analysis of concrete transport properties. Mater Struct 47(1):1–15. doi:10.1617/s11527- 013-0047-z
8. Conciatori D, Sadouki H, Brühwiler E (2008) Capillary suction and diffusion model for chloride ingress into concrete. Cement Concrete Res 38:1401–1408
9. Dagenais MG, Gaudry MJ, Cong Liem T (1987) Urban travel demand : the impact of box-cox transformations with nonspherical residual errors. Transp Res 21:443–477 CO- DEN TRBMDY
10. Davis, S.L., Goldberg, D.: Transportation for america—the fix we're in for: the state of our nation's bridges 2013 (2013). http://t4america.org/docs/bridgereport2013/2013Bridge Report.pdf. Accessed 03 Dec 2013
11. EU—Brite EuRam III (2000) Duracrete—final technical report general guidelines for durability design and redesign. Technical report, Document BE95-1347/R17.
12. Forbes C, Evans M, Hastings N, Peacock B (2011) Statistical distributions, Forth edn. John Wiley and Sons, Hoboken
13. Glasser F, Marchand J, Samson E (2008) Durability of concrete—degradation phenomena involving detrimental chemical reactions. Cement Concrete Res 38:226–246
    Henchi K, Samson E, Chapdelaine F, Marchand J (2007) Advanced finite-element predictive model for the service life prediction of concrete infrastructures in support of asset management and decision-making. In: Soibelman L et al (eds) ASCE computing in civil engineering. Pittsburgh, USA, pp 870–880
14. Henocq P, Samson E, Marchand J, Clark B (2007) Determination of the chloride content threshold to initiate steel corrosion. In: 5th International Essen Workshop—Transport in Concrete-Nanostructure and Macrostructure, Essen.
15. Jones M, Macphee D, Chudek J, Hunter G, Lannegrand R, Talero R, Scrimgeour S (2003) Studies using 27al mas nmr of afm and aft phases and the friedel's salt. Cement Concrete Res 33:177–182
16. Kreijger PC (1984) The skin of concrete composition and properties. Mater Struct 17:275–283
17. Larsen C, Sellevold E, Ostvik J, Vennesland O (2006) Electrical resistivity of concrete—part ii: Influence of moisture content and temperature. In: Marchand J et al. (eds) Advances in concrete through science and engineering, Quebec
18. Li YH (1974) Diffusion of ions in sea water and in deep-sea sediments. Geochim et Cosmochim Acta 38:703–714
19. Marchand J, Samson E (2009) Predicting the service-life of concrete structures—limitations of simplified models. Cement Concrete Compos 31:515–521
20. McDonald D, Pfeifer D, Sherman M (1998) Corrosion evaluation of epoxy-coated, metallic clad, and solid metallic reinforcing abrs in concrete. Technical report, Federal Highway Administration
21. Rosenblueth E (1975) Point estimates for probability moments. Proc Nat Acad Sci USA 72:3812–3814
22. Rosenblueth E (1981) Two-point estimates in probabilities. Appl Math Model 5:329–335
23. Samson E, Marchand J (2006) Multiionic approaches to model chloride binding in cementitious materials. In: 2nd International Symposium on Advances in Concrete through Science and Engineering, Quebec City.
24. Samson E, Marchand J (2007) Modeling the effect of temperature on ionic transport in cementitious materials. Cement Concrete Res 37:455–468
25. Samson E, Marchand J (2007) Modeling the transport of ions in unsaturated cement-based materials. Comput Struct 85:1740–1756
26. Samson E, Marchand J, Henocq P, BeausTjour P (2008) Recent advances in the determination of ionic diffusion coefficients using migration test results. In: 2nd International Conference on Concrete Modelling, Delft.
27. Suryavanshi A, Scantlebury J, Lyon S (1996) Mechanism of friedel's salt formation in cement rich in tri-calcium aluminate. Cement Concrete Res 26:717–727
28. Taheri-Motlagh A (1998) Durability of reinforced concrete structures in aggressive marine environment. Ph.D. thesis, Delft University of Technology, Delft.
29. UFGS (2010) United Facilities Guide Specifications (UFGS) 03 31 29. UFGS, USA.
30. US Environmental Protection Agency (2001) Risk assessment guidance for superfund: Vol iii—part a, process for conducting probabilistic risk assessment. Technical report, EPA 540-R-02-002.
31. USDOT, FHWA, FTA (2006) 2006 status of the nation's highways, bridges, and transit—condition & performance. Technical report, Report to congress.
32. USDOT, FHWA, FTA (2010) 2010 status of the nation's highways, bridges, and transit—condition & performance. Technical report, Report to congress.
33. Valley B, Kaiser P, Duff D (2010) Consideration of uncertainty in modelling the behaviour of underground excavations. In: 5th international seminar on deep and high stress mining, Santiago.
34. Zhang G, Zheng Z, Wan J (2005) Modeling reactive geochemical transport of concentrated aqueous solutions. Water Resources Research 41.